MRS Advances

X-Ray Diffraction and Electron Microscopy Studies of the Size Effects on Pressure-Induced Phase Transitions in CdS Nanocrystals

Lingyao Meng[1], Hongyou Fan[2,3,4], J. Matthew D. Lane[2], Luke Baca[1], Jackie Tafoya[1], Tommy Ao[2], Brian Stoltzfus[2], Marcus Knudson[2], Dane Morgan[5], Kevin Austin[2], Changyong Park[6], and Yang Qin[1]

[1]*Department of Chemistry and Chemical Biology, University of New Mexico, Albuquerque, New Mexico, United States*

[2]*Sandia National Laboratories, Albuquerque, New Mexico, United States*

[3]*Department of Chemical and Biological Engineering, University of New Mexico, Albuquerque, New Mexico, United States*

[4]*Center for Integrated Nanotechnology, Sandia National Laboratories, Albuquerque, New Mexico, United States*

[5]*Nevada National Security Site, New Mexico Operations-Sandia, Albuquerque, New Mexico, United States*

[6]*HPCAT, X-ray Science Division, Argonne National Laboratory, Lemont, Illinois, United States*

Abstract

In recent years, investigations of the phase transition behavior of semiconducting nanoparticles under high pressure has attracted increasing attention due to their potential applications in sensors, electronics, and optics. However, current understanding of how the size of nanoparticles influences this pressure-dependent property is somewhat lacking. In particular, phase behaviors of semiconducting CdS nanoparticles under high pressure have not been extensively reported. Therefore, in this work, CdS nanoparticles of different sizes are used as a model system to investigate particle size effects on high-pressure-induced phase

transition behaviors. In particular, 7.5, 10.6, and 39.7 nm spherical CdS nanoparticles are synthesized and subjected to controlled high pressures up to 15 GPa in a diamond anvil cell. Analysis of all three nanoparticles using in-situ synchrotron wide-angle X-ray scattering (WAXS) data shows that phase transitions from wurtzite to rocksalt occur at higher pressures than for bulk material. Bulk modulus calculations not only show that the wurtzite CdS nanomaterial is more compressible than rocksalt, but also that the compressibility of CdS nanoparticles depends on their particle size. Furthermore, sintering of spherical nanoparticles into nanorods was observed for the 7.5 nm CdS nanoparticles. Our results provide new insights into the fundamental properties of nanoparticles under high pressure that will inform designs of new nanomaterial structures for emerging applications.

INTRODUCTION

Semiconducting materials have attracted great interest over the past few decades because of their widespread applications in modern electronic and photonic devices. In particular, binary II-VI semiconductors (e.g., ZnS, CdS, CdSe, ZnO) have been shown to possess distinctive electronic and optoelectronic properties, such as wide ranges of direct band gaps with high electro-optic coefficients, making them excellent candidates for applications in solar cells, laser diodes, and light-emitting diodes [1,2]. Cadmium sulfide (CdS) is one of the most studied semiconducting materials in the II-VI family with a direct band gap of 2.53 eV. It has been extensively used as a photocatalysis, photoresistors, and window layer of junction solar cells [3-5]. Under normal conditions, CdS crystallizes into either cubic zinc blende (ZB) or hexagonal wurtzite (WZ) structures, with the WZ structure being slightly more thermodynamically stable. Another phase, rocksalt (RS), has been known to exist under high pressure [6]. In bulk CdS material, it has been reported that the phase transition from WZ to RS occurs at 2.6 GPa [7].

Recently, synthesis and characterization of nanomaterials of CdS have received increasing consideration due to their unique size- and shape-dependent physical and chemical properties. These properties have led to potential applications for CdS nanoparticles as biosensors, lasers, and solar cells [8-10]. Various methods have been described to synthesize CdS nanoparticles with different sizes and shapes [11-14]. As the surface area-to-volume ratio increases with decreasing particle size, some of the properties of nanoparticles, including their pressure responses, can be very different from their bulk counterparts. Achieving a better understanding of the high-pressure behaviors of nanoparticles can reveal valuable insights into their structural phase stability and mechanical properties; this knowledge will be useful in developing future multifunctional devices that can be used in high-pressure environments. Research has also shown that besides the atomic scale phase transition, applying high pressure can be used as a potential tool to manufacture nano-sized materials. For example, both metal and semiconductor spherical nanoparticles have been reported to sinter into nanowires under high pressure [15-26]. Such fine-tuned behaviors caused by controlled morphological changes under high pressure open new doors toward the design, synthesis and application of advanced nanomaterials.

Previous studies on high-pressure phase transition behaviors of CdS nanoparticles have shown that the WZ to RS phase transition of CdS nanoparticles occurs at elevated pressure in comparison to the bulk sample [27-29], which is in agreement with trends reported for other types of nanoparticles, and can be explained by the high surface energy of nanoparticles [30]. In addition to the nanosize effect, metal doping can also alter the phase transition properties of CdS nanoparticles. Prior research has revealed that doping with Eu^{3+} can increase the WZ to RS phase transition

pressure of CdS nanoparticles from 4.76 GPa to 5.22 GPa; while doping with Co^{2+} can reduce the ZB to RS phase transition pressure of CdS nanoparticles from 4.89 GPa to 4.06 GPa [31,32]. Other than these reports, investigations of how the nano-sizes of CdS nanoparticles affect this pressure-depended phase transition has been rarely reported and opposite trends have been observed. Mishara *et al.* [27] reported that the transition pressure decreased as the particle size increased from 10 nm to 44 nm; while Nanba *et al.* [29] claimed an increase in phase transition pressure with increasing CdS particle size from 40 nm to 400 nm. Furthermore, the size effect on pressure-induced morphology transition is also not well understood. Therefore, it is of general interest to explore the influence of CdS nanoparticle sizes on their high-pressure-induced properties in a systematic manner.

In this work, we have prepared spherical 7.5, 10.6, and 39.7 nm diameter CdS nanoparticles in the hexagonal WZ phase to study the size effect by using in-situ high-pressure wide-angle X-ray scattering (WAXS) measurements. In addition, we have studied the change of nanoparticle morphologies by transmission electron microscopy (TEM) before and after the high-pressure experiments. Furthermore, bulk moduli of different particles in different phases are calculated for comparison.

EXPERIMENTAL DETAILS

Synthesis of CdS Nanoparticles

The 7.5 nm and 10.6 nm spherical CdS nanoparticles were synthesized using the hot injection method following an established literature procedure [33]. The 39.7 nm spherical CdS nanoparticles were synthesized through hydrothermal process [34].

As-synthesized CdS nanoparticles were drop-casted (100 mg/mL in toluene) onto Si wafers to create nanoparticle thin films. A small part of the film was then carefully peeled off and loaded into the diamond anvil cell for (DAC) high-pressure characterizations.

Characterizations

Transmission electron microscopy (TEM) images were observed on a JEOL-2010F microscope operating at 220 kV. Room pressure powder X-ray diffraction (XRD) patterns were measured at ambient condition using a Rigaku Smartlab diffractometer with a Cu Kα beam (λ = 1.54 Å). In-situ high-pressure WAXS experiments were carried out at beamline 16-BM-D [35] of the Advanced Photon Source (APS), Argonne National Laboratory (ANL) with X-ray wavelength of λ = 0.41328 Å. A pair of diamond anvils was used to generate pressure up to 15 GPa with the flat diamond culets diameter of 300 μm. A rhenium gasket was pre-indented and laser drilled with a hole of 175 μm in diameter and 20 μm thick to serve as the sample chamber. A ruby ball was also loaded into the sample chamber to monitor the sample pressure using ruby fluorescence spectroscopy. Neon gas was used as the pressure transmitting medium. The exposure time was 30 s and the sample to detector distance was ~288.7 mm. The diffraction patterns were collected using a Mar345 Image Plate detector and integrated using the Dioptas software [36].

DISCUSSION

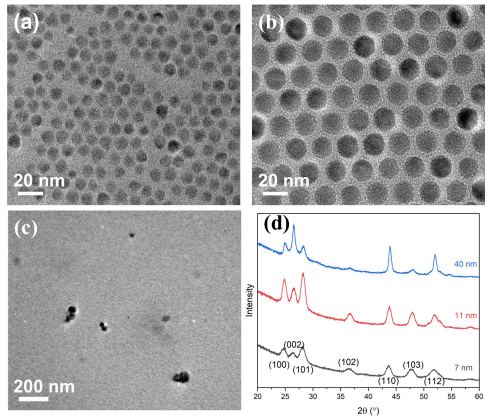

Figure 1. TEM images of (a) 7.5 nm, (b) 10.6 nm, (c) 39.7 nm CdS nanoparticles and (d) corresponding room pressure powder XRD spectrum.

Figure 1(a)-(c) are the TEM images of as-synthesized CdS nanoparticle samples with average size of 7.5±0.9, 10.6±1.2, and 39.7±6.6 nm, respectively. The crystalline phase structure of each sample at room pressure was then measured by XRD, as shown in Figure 1(d). The resulting XRD patterns show well resolved characteristic peaks of CdS hexagonal wurtzite phase (JCPDS card No. 75-1545).

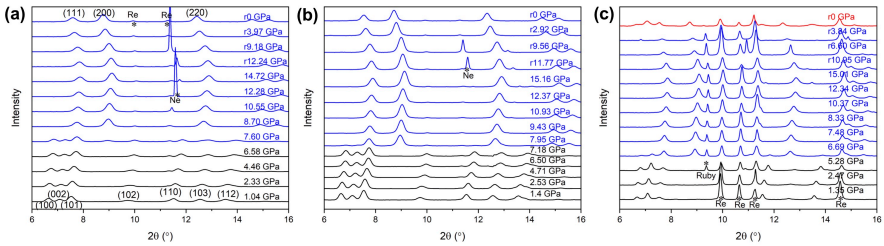

Figure 2. Representative synchrotron WAXS data during compression and decompression of (a) 7.5 nm, (b) 10.6 nm and (c) 39.7 nm CdS nanoparticles. r represents the releasing pressure, the black curve represents the WZ phase, the blue curve represents the RS phase, and the red curve represents a mixture of WZ and RS. Impurity peaks from gasket Re, neon gas and ruby are marked with asterisk.

Nanoparticles were then loaded into a DAC, and integrated synchrotron WAXS patterns for different samples during the compression and decompression process are displayed in Figure 2. It can be seen that all three samples possess the normal WZ structures at ambient pressure, and that with increasing pressure the corresponding diffraction peaks shifted to higher 2θ value (lower d-spacing) as the result of the unit cell contraction. With further increasing pressure, a new phase, characterized by the appearance of new peaks that are indexed as cubic RS phase (JCPDS card No. 21-829) appeared. The onset of WZ to RS phase transition pressure was measured to be 7.60, 7.95, and 6.69 GPa for the 7.5, 10.6, 39.7 nm samples, respectively. The RS phase was maintained up to 15 GPa, and then pressure was gradually released. For 7.5 nm and

10.6 nm samples, the RS phase was preserved when the pressure was released back to ambient, which represents an irreversible phase transition process. For the 39.7 nm sample, some of the wurtzite peaks reappeared at r0 GPa (the fully decompressed state), indicating that the phase transition process is partially reversible. Compared with bulk CdS, which shows reversible WZ to RS phase transition at about 2.6 GPa [7], CdS nanoparticles have higher phase transition pressures. 7.5 nm and 10.6 nm samples show similar WZ to RS phase transition pressure, while the phase transition pressure decreases with increasing the particle size from 10.6 nm to 39.7 nm. In the meantime, large particles tend to behave more like bulk material with partial reversible phase transition processes. These results indicate that the size of the particle can significantly affect both the phase transition pressure and the reversibility of the phase transition process. Similar size-dependent phase transition behavior has also been reported for other types of nanoparticles and can be explained by the increase of surface energy with decreasing particle size [37].

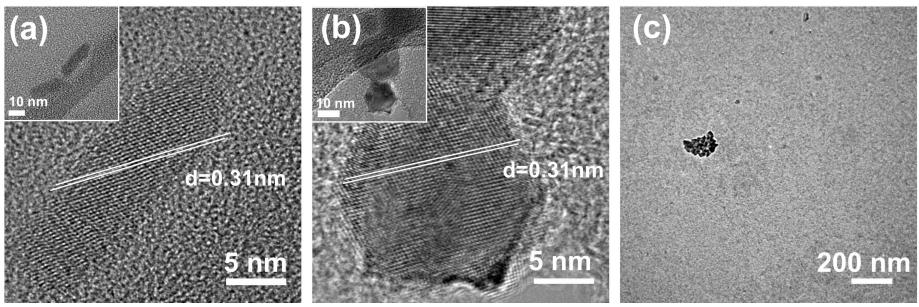

Figure 3. TEM images of (a) 7.5 nm, (b) 10.6 nm, and (c) 39.7 nm CdS nanoparticle samples after compression and decompression process.

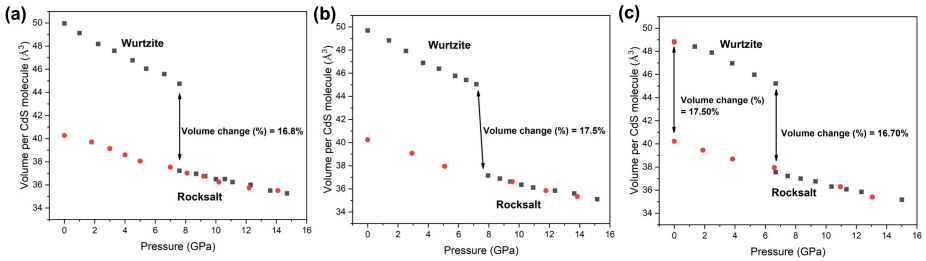

Figure 4. Dependence of unit cell volume on the applied external pressure for (a) 7.5, (b) 10.6, and (c) 39.7 nm CdS nanoparticles. Black dots represents the compression process and red dots represent the decompression process.

After the high-pressure experiments, CdS nanoparticle samples were collected and dissolved in toluene for TEM analysis. Figures 3 (a)–(b) are the lattice-resolved high-resolution TEM images for 7.5 and 10.6 nm samples for which the lattice can be determined to be the (111) cubic RS crystal diffraction plan with d-spacing equal to 0.31 nm. The insets in Figures 3 (a)–(b) show the overall sample morphologies. The solubility of the 39.7 nm sample was limited; therefore, no high-resolution TEM image was obtained. Comparing the TEM images, we see a sphere to a rod-like morphology transformation of the 7.5 nm sample that is not evident in the other two samples, and

this morphology transformation has not yet been observed in other high pressure studies of CdS nanoparticles. Previous studies have shown that ordered fcc close-packed-spherical nanoparticles can be transformed to hexagonal packed nanowires under high pressure [15-17], because, by increasing pressure, nanoparticles located along the pressure applying direction can easily contact one another and then consolidate into new nanostructures by nanoparticle coalescence. Our hypothesis is that even though nanoparticles are not closely packed in our experiments, some of the randomly arranged particles can still locate along the pressure applying direction. It has been demonstrated that particles with size $\leq$ 10 nm tend to sinter together to reduce their surface energy more than bigger particles [38], but whether bigger (e.g. 39.7 nm) nanoparticles can sinter or not is still not clear. The detailed mechanism of this morphology transformation is still being studied.

The unit cell volume change of different samples under pressure was calculated and summarized in Figure 4. From WZ to RS phase, about 17% volume decrease is calculated for all samples, close to the previously reported data [39]. Bulk modulus is an important mechanical property that denotes the stiffness of the material. Bulk moduli of different samples in different phases were then determined by fitting the 2nd order Birch-Murnaghan equation of state [40-42].

$$P=(3/2)B_0[(V_0/V)^{7/3}-(V_0/V)^{5/3}] \quad (1)$$

In this equation, B_0 and V_0 are the bulk modulus and initial unit cell volume at room pressure, respectively. V_0 can be calculated form the room pressure powder XRD data. The resulting bulk moduli are shown in Table 1.

Table 1. Unit cell volumes and bulk moduli of CdS nanoparticles.

Sample Size	Wurtzite (WZ)		Rocksalt (RS)	
	V_0 (Å^3)	B_0 (GPa)	V_0 (Å^3)	B_0 (GPa)
7.5 nm	99.92	57.49±0.93	161.10	85.14±0.59
10.6 nm	99.38	59.97±0.86	160.97	84.09±0.71
39.7 nm	97.69	78.90±5.02	161.10	84.36±0.46

Bulk moduli of nanoparticles at both the WZ and RS phases are higher when compared to the reported data of the bulk CdS material (B_0 = 54.0 GPa for WZ and B_0 = 68.0 GPa for RS [43]), which agrees with the trends observed for other types of particles [15,44,45]. In addition, we found that WZ nanoparticles show lower bulk modulus values than RS particles, indicating that they are more compressible. Also, for the WZ phase, the bulk modulus increases with increasing particle size, while those of RS nanoparticles remain similar to each other. A similar trend has been observed for γ-Fe_2O_3 [46] and PbS [47] nanoparticles, but the opposite behavior was also reported in ZnS nanoparticles [48]. Our results are contrary to those in prior studies, but the particles studied previously were of different size ranges and covered by different surfactants. Therefore, there is still no agreement on how the size of the particle affects the value of the bulk modulus, and our results cannot be considered as a general trend in nanoparticles.

CONCLUSIONS

In summary, the impact of nanoparticle size on high-pressure-induced phase transitions were studied using spherical CdS nanoparticles having average sizes of 7.5, 10.6, and 39.7 nm. Synchrotron WAXS analysis shows unique size-dependent phase

transition pressure and phase transition reversibility. It was revealed that the WZ to RS phase transition pressure increased with increasing particle size from 10.6 nm to 39.7 nm. Also, morphology transformation from sphere to rod was observed after the compression-decompression cycle only for the 7.5 nm sample. Further calculations of the bulk modulus shows that for WZ CdS nanoparticles, bulk modulus increases with increasing particle size. With CdS as the model material, our work provides detailed information about the effects of particle size on their high-pressure behavior, and it may help to initiate new approaches to designing nanoparticles for high-pressure applications.

ACKNOWLEDGMENTS

This was supported by the National Science Foundation (DMR-1453083 and CHE-1904659) and research reported in this publication was supported by an Institutional Development Award (IDeA) from the National Institute of General Medical Sciences of the National Institutes of Health under grant number P20GM103451.This work was supported by the Sandia's Laboratory Directed Research & Development (LDRD) program. This paper describes objective technical results and analysis. Portions of this work were performed at HPCAT (Sector 16), Advanced Photon Source (APS), Argonne National Laboratory. HPCAT operations are supported by DOE-NNSA's Office of Experimental Sciences. The Advanced Photon Source is a U.S. Department of Energy (DOE) Office of Science User Facility operated for the DOE Office of Science by Argonne National Laboratory under Contract No. DE-AC02-06CH11357. Any subjective views or opinions that might be expressed in the paper do not necessarily represent the views of the U.S. DOE or the United States Government. Research was carried out, in part, at the Center of Integrated Nanotechnology (CINT), a US Department of Energy, Office of Basic Energy Sciences user facility. Sandia National Laboratories is a multimission laboratory managed and operated by National Technology and Engineering Solutions of Sandia, LLC., a wholly owned subsidiary of Honeywell International, Inc., for the U.S. Department of Energy's National Nuclear Security Administration under contract DE-NA0003525. This manuscript has been authored by Mission Support and Test Services, LLC, under Contract No. DE-NA0003624 with the U.S. Department of Energy, National Nuclear Security Administration, Office of Defense Programs and supported by the Site-Directed Research and Development Program. The United States Government retains and the publisher, by accepting the article for publication, acknowledges that the United States Government retains a non-exclusive, paid-up, irrevocable, worldwide license to publish or reproduce the published form of this manuscript, or allow others to do so, for United States Government purposes. The U.S. Department of Energy will provide public access to these results of federally sponsored research in accordance with the DOE Public Access Plan (http://energy.gov/downloads/doe-public-access-plan).

REFERENCES

1. M. Afzaal and P. O'Brien, *J. Mater. Chem* **16**, 1597 (2006).
2. H. E. Ruda, *Widegap II–VI compounds for opto-electronic applications*. (Springer Science & Business Media, 2013).
3. Q. Zhang, X. Guo, X. Huang, S. Huang, D. Li, Y. Luo, Q. Shen, T. Toyoda and Q. Meng, *Phys. Chem. Chem. Phys.* **13**, 4659 (2011).
4. L. Cheng, Q. Xiang, Y. Liao and H. Zhang, *Energy Environ. Sci.* **11**, 1362 (2018).
5. J. Liu, Y. Liang, L. Wang, B. Wang, T. Zhang and F. Yi, *Mat. Sci. Semicon. Proc.* **56**, 217 (2016).
6. A. F. Wells, *Structural inorganic chemistry*. (Oxford university press, 2012).

7. N. Owen, P. Smith, J. Martin and A. Wright, *J. Phys. Chem. Solids* **24**, 1519 (1963).
8. R. N. Mitra, M. Doshi, X. Zhang, J. C. Tyus, N. Bengtsson, S. Fletcher, B. D. Page, J. Turkson, A. J. Gesquiere and P. T. Gunning, *Biomaterials* **33**, 1500 (2012).
9. J. Zhang, D. Li, R. Chen and Q. Xiong, *Nature* **493**, 504 (2013).
10. Y. Wang, H. Fu, Y. Wang, L. Tan, L. Chen and Y. Chen, *Phys. Chem. Chem. Phys.* **18**, 12175 (2016).
11. K.-T. Yong, Y. Sahoo, M. T. Swihart and P. N. Prasad, *J. Phys. Chem. C* **111**, 2447 (2007).
12. P. Zhang and L. Gao, *Langmuir* **19**, 208 (2003).
13. W.-S. Chae, H.-W. Shin, E.-S. Lee, E.-J. Shin, J.-S. Jung and Y.-R. Kim, *J. Phys. Chem. B* **109**, 6204 (2005).
14. H. Chu, X. Li, G. Chen, W. Zhou, Y. Zhang, Z. Jin, J. Xu and Y. Li, *Cryst. Growth Des.* **5**, 1801 (2005).
15. B. Li, X. Wen, R. Li, Z. Wang, P. G. Clem and H. Fan, *Nat. Commun.* **5**, 4179 (2014).
16. H. Wu, F. Bai, Z. Sun, R. E. Haddad, D. M. Boye, Z. Wang and H. Fan, *Angew. Chem. Int. Ed.* **49**, 8431 (2010).
17. B. Li, K. Bian, X. Zhou, P. Lu, S. Liu, I. Brener, M. Sinclair, T. Luk, H. Schunk, L. Alarid and H. Fan, *Sci. Adv.* **3**, e1602916 (2017).
18. F. Bai, K. Bian, X. Huang, Z. Wang and H. Fan, *Chem. Rev.* (2019).
19. H. Wu, F. Bai, Z. Sun, R. E. Haddad, D. M. Boye, Z. Wang, J. Y. Huang and H. Fan, *J. Am. Chem. Soc.* **132**, 12826 (2010).
20. Z. Wang, C. Schliehe, T. Wang, Y. Nagaoka, Y. C. Cao, W. A. Bassett, H. Wu, H. Fan and H. Weller, *J. Am. Chem. Soc.* **133**, 14484 (2011).
21. W. Li, H. Fan and J. Li, *Nano Lett.* **14**, 4951 (2014).
22. H. Wu, Z. Wang and H. Fan, *J. Am. Chem. Soc.* **136**, 7634 (2014).
23. Z. Wang, X.-D. Wen, R. Hoffmann, J. S. Son, R. Li, C.-C. Fang, D.-M. Smilgies and T. Hyeon, *Proc. Natl. Acad. Sci. U.S.A.* **107**, 17119 (2010).
24. Z. Wang, O. Chen, C. Y. Cao, K. Finkelstein, D.-M. Smilgies, X. Lu and W. A. Bassett, *Rev. Sci. Instrum.* **81**, 093902 (2010).
25. H. Zhu, Y. Nagaoka, K. Hills-Kimball, R. Tan, L. Yu, Y. Fang, K. Wang, R. Li, Z. Wang and O. Chen, *J. Am. Chem. Soc.* **139**, 8408 (2017).
26. Y. Nagaoka, K. Hills-Kimball, R. Tan, R. Li, Z. Wang and O. Chen, *Adv. Mater.* **29**, 1606666 (2017).
27. A. Mishra, N. Garg, K. Pandey and V. Singh, *J. Phys.: Conf. Ser.* **377**, 12012 (2012).
28. R. Martín-Rodríguez, J. González, R. Valiente, F. Aguado, D. Santamaría-Pérez and F. Rodríguez, *J. Appl. Phys.* **111**, 063516 (2012).
29. T. Nanba, M. Muneyasu, N. Hiraoka, S. Kaga, G. Williams, O. Shimomura and T. Adachi, *J. Synchrotron Radiat.* **5**, 1016 (1998).
30. S. H. Tolbert and A. Alivisatos, *Annu. Rev. Phys.* **46**, 595 (1995).
31. R. Zhao, T. Yang, Y. Luo, M. Chuai, X. Wu, Y. Zhang, Y. Ma and M. Zhang, *RSC Adv.* **7**, 31433 (2017).
32. R. Zhao, P. Wang, B. Yao, T. Hu, T. Yang, B. Xiao, S. Wang, C. Xiao and M. Zhang, *RSC Adv.* **5**, 17582 (2015).
33. V. Arora, U. Soni, M. Mittal, S. Yadav and S. Sapra, *Journal of colloid and interface science* **491**, 329 (2017).
34. Y. Fang, Z. Li, Y. Jiang, X. Wang, H.-Y. Chen, N. Tao and W. Wang, *Proc. Natl. Acad. Sci. U.S.A.* **114**, 10566 (2017).
35. C. Park, D. Popov, D. Ikuta, C. Lin, C. Kenney-Benson, E. Rod, A. Bommannavar and G. Shen, *Rev. Sci. Instrum.* **86**, 072205 (2015).
36. C. Prescher and V. B. Prakapenka, *High Pressure Research* **35**, 223 (2015).
37. Q.-J. Li and B.-B. Liu, *Chin. Phys. B* **25**, 076107 (2016).
38. C. Guozhong, *Nanostructures and nanomaterials: synthesis, properties and applications*. (World scientific, 2004).
39. J. Kennedy and W. Benedick, *J. Phys. Chem. Solids* **27**, 125 (1966).
40. F. D. Murnaghan, *Amer. J. Math.* **59**, 235 (1937).
41. F. Birch, *Phys. Rev.* **71**, 809 (1947).
42. F. Murnaghan, *Proc. Natl. Acad. Sci. U.S.A.* **30**, 244 (1944).
43. M. Grünwald, A. Zayak, J. B. Neaton, P. L. Geissler and E. Rabani, *J. Chem. Phys.* **136**, 234111 (2012).
44. J. Jiang, J. S. Olsen, L. Gerward and S. Mørup, *EPL* **44**, 620 (1998).

45. Q. Gu, G. Krauss, W. Steurer, F. Gramm and A. Cervellino, *Phys. Rev. Lett.* **100**, 045502 (2008).
46. S. Clark, S. Prilliman, C. Erdonmez and A. Alivisatos, *Nanotechnology* **16**, 2813 (2005).
47. K. Bian, W. Bassett, Z. Wang and T. Hanrath, *J. Phys. Chem. Lett* **5**, 3688 (2014).
48. B. Gilbert, H. Zhang, B. Chen, M. Kunz, F. Huang and J. Banfield, *Phys. Rev.* **74**, 115405 (2006).